Journal of Inorganic Biochemistry 148 (2015) 35–48

Contents lists available at ScienceDirect

Journal of Inorganic Biochemistry

journal homepage: www.elsevier.com/locate/jinorgbio

Sunflower metallothionein family characterisation. Study of the Zn(II)- and Cd(II)-binding abilities of the HaMT1 and HaMT2 isoforms

M. Tomas [a,b], M.A. Pagani [c], C.S. Andreo [c], M. Capdevila [a], S. Atrian [b], R. Bofill [a,*]

[a] Departament de Química, Facultat de Ciències, Universitat Autònoma de Barcelona, 08193 Cerdanyola del Vallès, Barcelona, Spain
[b] Departament de Genètica, Facultat de Biologia, Universitat de Barcelona, Av. Diagonal 645, 08028 Barcelona, Spain
[c] Centro de Estudios Fotosintéticos y Bioquímicos, CONICET, Suipacha 531, 2000 Rosario, Argentina

ARTICLE INFO

Article history:
Received 17 November 2014
Received in revised form 21 February 2015
Accepted 22 February 2015
Available online 28 February 2015

Keywords:
Sunflower
Metallothionein
Plant MT
Zn-binding
Cd-binding
Biological function

ABSTRACT

Plant metallothioneins (MTs) constitute a family of small Cys-rich proteins capable of coordinating metal ions, significantly differing from microbial and animal MTs. They are divided into four subfamilies depending on the Cys pattern in their sequence. In this work, the MT system of the sunflower plant (*Helianthus annuus*) has been defined, with ten genes coding for MTs (*HaMT*) belonging to the four plant MT subfamilies; three HaMT1, four HaMT2, one HaMT3 and two HaMT4 isoforms. The gene expression pattern and capacity to confer metal resistance to yeast cells have been analysed for at least one member of each subfamily. The divalent metal ion-binding abilities of HaMT1-2 and HaMT2-1 (the isoforms encoded by the most abundantly expressed *HaMT1* and *HaMT2* isogenes) have been characterised, as HaMT3 and HaMT4 were previously studied. Those isoforms constitute an optimum material to study the effect of Cys number variability on their coordination abilities, as they exhibit additional Cys residues regarding the canonical Cys pattern of each subfamily. Our results show that the variation in the number of Cys does not drastically modify their M(II)-binding abilities, but instead modulates the degree of heterogeneity of the corresponding recombinant syntheses. Significantly, the Zn(II)–HaMT1 complexes were highly susceptible to proteolytic cleavage. The recombinant Cd–MT preparations of both isoforms exhibit significant acid-labile sulphide content-Cd_6S_8 or Cd_7S_7 species. Overall results suggest that HaMT2-1 is probably associated with Cd(II) detoxification, in contrast to HaMT1-2, which may be more related to physiological functions, such as metal ion transport and delivery.

1. Introduction

Since the first metallothionein (MT) was discovered in horse kidney in 1957 [1], much has been done to study this superfamily of Cys-rich, low molecular weight, metalloproteins that bind heavy metal ions. These peculiar proteins lack secondary and tertiary structure elements in their metal-free (or apo) forms – with the exception of the long Cys-free regions of plant MTs, where β-sheet structural elements have been detected [2] – from which it becomes evident that metal binding dictates their final 3D features through the formation of metal-thiolate clusters. Nowadays, it is widely accepted that they are mainly involved in metal homeostasis and detoxification, as well as in protection against oxidative stress [3]. MTs are present in almost all living organisms, but they show highly diverse amino acid sequences. Thus, a classification depending on taxonomic criteria has been proposed [4]. Family 1 (vertebrate) MTs, and among them, mammalian MTs in particular, have been the most studied since their discovery more than 50 years ago, with their $M(II)_3$–$(SCys)_9$ and $M(II)_4$–$(SCys)_{11}$ clusters being used as models for metal ion coordination in divalent metal–MT complexes. In contrast, the first plant MT (family 15) was discovered in wheat (*Triticum aestivum*) embryos just 30 years ago, in 1983 [5].

Despite the fact that the number of MT sequences identified in plants is continually increasing, the wide variability in their amino acid sequences, and also if compared to vertebrate MTs, mean that there are insufficient data available to successfully analyse the relationships between their metal-binding properties and their potential biological functions. This high sequence heterogeneity is the reason why family 15 MTs have been divided into four subfamilies, depending on the number and distribution of their Cys residues [6]. Ec-1, the aforementioned wheat MT, belongs to subfamily MT4, and until now it is the only native plant MT isolated, as well as the only plant MT for which a 3D structure, that of the Zn(II)–Ec-1 complex, has been solved [7,8]. As regards MT1, MT2 and MT3 subfamilies, their sequences dramatically diverge from those of subfamily MT4. They present two Cys-rich regions separated by a Cys-free region (called *linker* or *spacer*), whereas MT4 subfamily shows two linkers between three Cys-rich regions.

More than 30 *MT-like* nucleotide sequences of subfamily 1 have been identified and their expression patterns analysed, but information at the protein level is still scarce [cf. recent review in 9]. MT1 canonical sequence contains six Cys residues both in its N-terminal and C-terminal

* Corresponding author. Tel.: +34 93 5812886; fax: +34 93 5812477.
E-mail address: Roger.Bofill@uab.cat (R. Bofill).

http://dx.doi.org/10.1016/j.jinorgbio.2015.02.016
0162-0134/

Cys-rich regions, but several variants with one or two extra Cys in the N-term domain are known (Table S1). The divalent metal-binding capacities of five MTs belonging to this subfamily have already been determined. Hence, the pea (*Pisum sativum*) PsMT-A isoform was found to coordinate 5.8 Cd(II) ions when heterologously synthesised in metal-enriched *Escherichia coli* cultures in the form of a glutathione-S-transferase (GST)-fusion protein [10]; 4 Cd(II) ions were found to be bound in wheat (*Triticum durum*) GST–dMT [11]; GST–OsMTI-1b from rice (*Oryza sativa*) coordinated 4.8 Cd(II) and 1.8 Zn(II) ions when reconstituted from its apo-form [12]; chickpea (*Cicer arietinum*) cicMT1 showed to bind up to 5 Zn(II) or Cd(II) ions [13]; and GmMT1 from soybean (*Glycine max*) contained an average of 3.8 Zn(II) ions and 8.1 Cd(II) ions per molecule when heterologously synthesised [14].

In contrast to MT1, a considerable amount of data has been reported for the members of the MT2 subfamily, as such that the number of *MT2* gene sequences in data banks doubles that of *MT1*. The archetypal MT2 proteins feature eight Cys residues at their N-term Cys-rich region with a unique –Cys–Cys– motif not present in any other plant MT subfamily, and six Cys residues at their C-term domain, but again variations on the number of Cys residues exist (Table S2). Since the N-term Cys residues are highly conserved, this subfamily is further divided into several subtypes according to the arrangement of the Cys residues in the C-terminal domain [15,16]. Reported divalent metal-binding properties of recombinant plant MT2s showed their ability to bind 3.6 Zn(II) ions in the case of watermelon (*Citrullus lanatus*) ClMT2 [17], 3.5 Zn(II) and 5.3–6.5 Cd(II) ions for cork oak (*Quercus suber*) QsMT [18,19], 5 Zn(II) and 5 Cd(II) ions for chickpea (*C. arietinum*) cicMT2 [20], and 4.3 Zn(II) as well as 6.7 Cd(II) ions for soybean (*G. max*) GmMT2 [14].

Sunflower (*Helianthus annuus*) is a vegetable crop cultivated mainly for its oil content, being among the four major sources of vegetable oil in the world [21]. Sunflower seeds contain from 39% to 49% highly nutritional oil – consisting of more than 90% of oleic and linoleic acid – and about 24% to 28% protein. Seeds are also rich in vitamins and nutrient minerals, such as calcium, iron, manganese, zinc, magnesium and selenium, but they also tend to accumulate toxic elements like cadmium, lead, and mercury [22]. Therefore, sunflower plants are being tested for phytoextraction applicability, i.e. remediation of metal-contaminated soils [23,24], since their high biomass production may improve the economic balance of phytoremediation if using sunflower oil for technical purposes. In this context, MTs are major candidates to be one of the determinants for the high metal accumulation properties of sunflower, and therefore their full characterisation may be useful to improve their environmental remediation applicability.

In this work we have screened expressed sequence tag (EST) and genomic databases to uncover all the genes of the sunflower MT family, with their sequences being comprehensively reported for the first time in this work. We have also determined their expression levels using quantitative real time PCR analysis. We have also performed phenotypic rescue experiments in *Saccharomyces cerevisiae* as an approximation of the physiological activity of one member of each subfamily of plant MTs, as well as the analysis of the divalent metal-binding abilities of one MT1 (HaMT1-2) and one MT2 (HaMT2-1) sunflower MT isoforms. Besides representing the *HaMT1* and *HaMT2* most highly expressed isogenes in sunflower, their corresponding peptides show the peculiarity of constituting a variant of plant MT1 and MT2 canonical sequences because of the presence of extra Cys residues, thus enhancing the interest of the study of their metal-binding properties. The characterisation of their Zn(II)- and Cd(II)-complexes, both obtained by recombinant synthesis in metal-enriched cultures (in vivo complexes), and the latter also by Zn/Cd exchange (in vitro complexes) has been performed through spectroscopic and spectrometric techniques. The potential consequences arising from the variations in the number of Cys residues from the canonical MT1 and MT2 sequences are also discussed in this work.

2. Experimental section

2.1. In silico identification of sunflower MTs

To obtain sunflower MT coding sequences, the NCBI EST library database was screened using *blastn* in the Basic Local Alignment Search Tool (BLAST) and the *Arabidopsis thaliana* metallothionein cDNA sequences NM_100633.2 (MT1a), NM_111773.3 (MT2a), NM_112401.1 (MT3) and NM_127888.1 (MT4a) as queries. From all the retrieved *H. annuus* ESTs, those present in collections from different sources or present in different genetic backgrounds were selected to continue the study. Clones DY927795 (HaMT1-1), DY927283 (HaMT1-2), DY931085 (HaMT2-1), DY931060 (HaMT2-2), BQ910832 (HaMT2-3) DY927914 (HaMT3) and BQ975039 (HaMT4-1) were purchased from the University of Arizona (The Compositae Genome Project). Upon signature of a Material Transfer Agreement (MTA) with the University of British Columbia, access to the Reference Genome of Sunflower, line HA412: Version 0.2 assembly was obtained during the course of this work. The search for sunflower MT genes was reassessed with the blast alignment tool using the seven previously selected cDNA HaMT sequences as queries.

2.2. Quantitative real time PCR (q-RT-PCR)

An analysis was made of three biological replicates, with each sample consisting of leaves, roots or seeds – 21 days postanthesis – pooled from three sunflower plants *cv*. VandeHaver grown in pots for 90 days. Total RNA was isolated with TRIZOL Reagent (Invitrogen) following the manufacturer's protocol and treated with DNase I (Fermentas). The cDNA was synthesised using an oligo (dT_{18}) primer from 1 μg of total RNA with the reverse transcriptase RevertAid (Fermentas) and RNaseOUT Recombinant RNase Inhibitor (Invitrogen). Quantitative real-time PCR reactions were performed in a 20-μL reaction volume with 0.5 μM and 0.2 μM gene-specific primers and probes, respectively (listed in Table 1), 2 μL of 1/100 diluted cDNA as a template, and LightCycler 480 Probes Master (Roche) as reaction mix. Sunflower actin (GenBank Accession AF282624), HaACT, was used as a reference gene. The amplicon lengths were 120 bp for HaMT1-1, 77 bp for HaMT1-2, 65 bp for HaMT2-1, 77 bp for HaMT2-2, 74 bp for HaMT2-3, 65 bp for HaMT3, 60 bp for HaMT4, and 68 bp for HaACT. The reactions were performed in a LightCycler 480 Instrument I qPCR System (Roche) in triplicate (technical replicates). PCR conditions were: 95 °C for 5 min, followed by 45 cycles of 95 °C for 10 s, 55 °C for 10 s, and 72 °C for 1 s. The fluorescence signal was determined for each cycle at the end of the extension step. The fold-change in gene expression was calculated using the comparative Ct method ($2^{-\Delta Ct}$) [25]. The amplification correlation coefficient, determined from serial dilutions, was 0.996 for HaMT1-1, 0.998 HaMT1-2, 0.995 for HaMT2-1, 0.999 for HaMT2-2, 0.995 for HaMT2-3, 0.999 for HaMT3, and 0.999 for HaMT4 and HaACT.

2.3. S. cerevisiae metal tolerance assays

For metal tolerance assays, two metal sensitive strains compatible with the use of the yeast expression vector p424 [26] were used: 51.2cΔc5 (MATa trp1-1 ura3-52 ade-his-CAN^R gal1 leu2-3112 met13 cup1::URA3 crs5::LEU2) devoid of any MT gene [27] and CM104 (MATa can1-100 his3-11 leu2-3112 trp1-1 ura 3-52 zrc1::HIS3 cot1::URA3) defective for vacuolar Zn transporters [28] and therefore zinc sensitive. Yeast expression vectors p424–HaMT were constructed as follows: HaMT coding regions were excised from vectors retrieved from the corresponding University of Arizona clones by digestion with *BamH*I/XhoI enzymes and ligated into p424 vector, thus remaining under the transcriptional control of the yeast GPD (glyceraldehyde-3-phosphate dehydrogenase) constitutive promoter. The p424 vector also contains the CYC1 (cytochrome c oxidase) terminator, the 2 μ replication origin, and the TRP1 (tryptophan) marker. Vector constructions p424–CUP1

Table 1
Sequence of the oligonucleotides and numbers of Universal Library Probes (Roche) used for qPCR assays.

	Direct oligonucleotide	Probe		Reverse oligonucleotide
Name	Sequence	Number	Name	Sequence
HaMT1-1 F	5′- GAGAAGTCGACCACCACCA	#161	*HaMT1-1 R*	5′- GCTTGATCCACAGCTGCAC
HaMT1-2 F	5′- TGTTGCACCCAGGATGACT	#73	*HaMT1-2 R*	5′- AGCTACTTCCGCACTTGCAC
HaMT2-1 F	5′- TGCAGCTGCTAAGGATCAAG	#165	*HaMT2-1 R*	5′- AAACATAATTCAAACACTGCTGCT
HaMT2-2 F	5′- TGGTTTGGATTTATGTTGGAGTT	#157	*HaMT2-2 R*	5′- ACACGACAAACCATTCAAATACTC
HaMT2-3 F	5′- ACCCACCACAGCCGTTAC	#164	*HaMT2-3 R*	5′- GATGTCGTCTTCTTGCTGTGG
HaMT3 F	5′- ACCCACCACAGCCGTTAC	#82	*HaMT3 R*	5′- TTTTCAGCTGCAGGAACCTC
HaMT4 F	5′- ACATCATTAGAAGCGATGAGGTC	#27	*HaMT4 R*	5′- TTCCCCTATTGAGGAACTGAAA
HaACT F	5′- GGAAGGACCTTTACGGTAACATT	#138	*HaACT R*	5′- CCTGTCAGCTATACCAGGGAAC

and p424–mMT1, respectively encoding for the yeast Cu-thionein Cup1 and the mouse MT1 isoforms, were used as controls [29]. Vector p424 and the p424–MT constructs were introduced into 51.2cΔc5 and CM104 cells using the lithium acetate procedure [30] and transformed cells were selected by their capacity to grow in complete synthetic medium (SC), lacking Trp (SC–Trp). For the functional complementation experiments, cultures of 51.2cΔc5 cells carrying either p424 or p424–MT were grown in SC–Trp liquid medium at 30 °C and 250 rpm, until OD600 = 0.5. Three or four 10-fold dilutions were performed, and 3 μL of each dilution were spotted on SC plates and on SC supplemented with copper, zinc or cadmium. Plates were incubated for 3 days at 30 °C and then photographed.

2.4. MT expression vectors construction

The HaMT1-2 and HaMT2-1 cDNAs were sub-cloned into the pGEX-4T1 vector (GE Healthcare) in order to obtain the pGEX–HaMT1-2 and pGEX–HaMT2-1 expression plasmids, respectively. Flanking *BamH*I/*Xho*I restriction sites were added by PCR amplification using the following oligonucleotides: 5′-CCGGGATCCATGTCTTGCTCAAGTGGAAAGTG-3′ as upstream primer and 5′-ATTCTCGAGTCAGCAGTTGCAAGGATCGCA CT-3′ as downstream primer for *HaMT1-2*; 5′-CACGGATCCATGTCTTGC TGCAGC-3′ as upstream primer and 5′-TCTCTCGAGTTAGCAGCTGCAG TTG-3′ as downstream primer for *HaMT2*. All the PCR reactions consisted of 35-cycle amplifications performed with 1.25 U of GoTaq DNA polymerase (Promega), 0.25 mM dNTPs and 0.20 μM of the required primers at 2 mM $MgCl_2$ (final concentration), in a final volume of 100 μL, under the following cycle conditions: 30 s at 94 °C (denaturation), 30 s at 55 °C (hybridisation), and 30 s at 72 °C (elongation). An initial denaturation step, where samples were heated at 94 °C for 5 min, ensured the complete denaturation of the target DNA, and elongation conditions were maintained for 7 min after the 35 cycles. The final products were analysed by agarose gel electrophoresis/GelRed Nucleic Acid Gel Stain (Biotium) staining, and the band with the expected size was excised and sub-cloned into the pGEX-4T1 vector. All the constructs were confirmed by automated DNA sequencing. To this end, the pGEX-derived constructs were transformed into *E. coli* MATCH I cells, and sequenced using the ABI PRISM BigDye Terminator v3.1 Cycle Sequencing Kit (Applied Biosystems) in an ABI PRISM 310 Automatic Sequencer (Applied Biosystems).

2.5. Recombinant synthesis and purification of MTs

Firstly, HaMT–GST fusion polypeptides were biosynthesised in 3 mL-cultures of transformed *E. coli* cells (BL21 strain). Expression was induced with isopropyl ß-D-thiogalactopyranoside (IPTG) and was allowed to grow for a further 3 h. Cells were harvested by centrifugation, re-suspended in 150 μL PBS buffer, and lysed by sonication. The total protein extract was analysed in 15% SDS-PAGE gels. Secondly, HaMT–GST fusion polypeptides were biosynthesised in 5 L-cultures of transformed *E. coli* cells (BL21 strain). Expression was induced with IPTG, and cultures were supplemented with final concentrations of 300 μM $ZnCl_2$ or 300 μM $CdCl_2$, and were allowed to grow for a further 3 h. Total protein extract was prepared from these cells as previously described [31]. Metal complexes were recovered from the fusion constructs by thrombin cleavage and batch-affinity chromatography using Glutathione-Sepharose 4B (GE Healthcare). After concentration using Centriprep Microcon 3 (Amicon), the metal complexes were finally purified through fast protein liquid chromatography (FPLC) in a Superdex 75 column (GE Healthcare) equilibrated with 50 mM Tris–HCl, pH 7.0. Selected fractions were confirmed by electrospray ionisation mass spectrometry (ESI-MS) (see conditions in next section) and kept at −80 °C until further use. All procedures were performed using Ar (pure grade 5.6) saturated buffers. Further details on the purification procedure specific for recombinant plant MTs can be found in previous works [19,32]. As a consequence of the cloning procedure, the dipeptide Gly–Ser is added to the N-terminus of the corresponding MT polypeptides. This minor modification of the native form was previously shown not to alter any of the MT metal-binding properties [33].

2.6. Spectroscopic and spectrometric characterisation of the M(II)–HaMT complexes

The S, Zn and Cd contents of all the M(II)–MT preparations were analysed by means of inductively coupled plasma atomic emission spectroscopy (ICP-AES) in a Polyscan 61E (Thermo Jarrell Ash) spectrometer, measuring S at 182.040 nm, Zn at 213.856 nm and Cd at 228.802 nm. Samples were treated as previously reported [34], but were alternatively incubated in 1 M HNO_3 at 65 °C for 10 min prior to measurements in order to eliminate possible traces of acid-labile sulphide ions, as previously described [35]. Protein concentrations were calculated from the acidic ICP-AES sulphur measurements, assuming that all S atoms were contributed by the MT peptide.

Molecular mass determinations were performed by ESI–TOF (time-of-flight)-MS on a Micro TOF-Q instrument (Bruker) interfaced with a 1100 Series HPLC Agilent pump, equipped with an auto sampler, all of them controlled by the Compass Software. Calibration was attained with ESI-L low concentration tuning mix (Agilent Technologies). Samples containing MT complexes were analysed under the following conditions: 20 μL of protein solution injected through a PEEK (polyether ether ketone) tubing (1.5 m × 0.18 mm i.d.), at 40 $\mu L \cdot min^{-1}$; capillary counter-electrode voltage of 5 kV; desolvation temperature at 90–110 °C; dry gas of 6 $L \cdot min^{-1}$; and spectra collection range of 800–2000 m/z. The carrier buffer was a 5:95 mixture of acetonitrile:ammonium acetate/ammonia (15 mM, pH 7.0). For analysis of the sequences of all recombinant MTs, 20 μL of the corresponding Zn–MT samples were injected under the same conditions described before, but using a 5:95 mixture of acetonitrile:formic acid pH 2.4 as liquid carrier, which caused the complete demetallation of the peptides.

A Jasco spectropolarimeter (Model J-715) interfaced to a computer (J700 software) was used for CD recording at a constant temperature of 25 °C maintained by a Peltier PTC-351S apparatus. Electronic absorption measurements were performed on an HP-8453 Diode array UV-visible spectrophotometer. All spectra were recorded with 1 cm capped quartz cuvettes, corrected for the dilution effects and processed using the GRAMS 32 Software.

2.7. Cd(II) addition to Zn(II)–MT complexes and acidification–reneutralisation of Cd(II)–MTs

For the Zn/Cd replacement studies, 15–20 μM preparations of the Zn(II)–MT complexes were treated with incremental amounts of $CdCl_2$ (1–9 Cd(II) eq) at pH 7. CD and UV spectra were recorded immediately after the metal addition and 10 min later, until invariant spectra were obtained. For the acidification–reneutralisation studies, 10–20 μM preparations of the Cd(II)–MT complexes were acidified from pH 7 to pH 2 with incremental volumes of diluted HCl solutions, and after that were reneutralised with diluted NaOH. CD, UV and ESI-MS spectra were recorded at selected steps. Oxygen-free conditions were maintained by saturation of all solutions with Ar during all experiments.

3. Results

3.1. In silico search for sunflower MTs

At the beginning of this study, no comprehensive information was available for the sunflower MT family members, either at the protein or gene level, so we took advantage of different databases to analyse the composition of the *H. annuus* MT system using in silico approaches. The screening of the sunflower NCBI EST database retrieved seven sequences, assignable to the four plant MT subfamilies. Two ESTs, named *HaMT1-1* and *HaMT1-2*, coded for MT1 peptides; and three, named *HaMT2-1*, *HaMT2-2* and *HaMT2-3*, for MT2 forms. One further EST was identified for the MT3 subfamily, and also a single EST was retrieved for MT4. These two latter cDNAs were respectively named *HaMT3* and *HaMT4*, and the corresponding HaMT3 and HaMT4 peptides were recently analysed in a separate study devoted to His-containing plant MTs [36].

During the course of this work, the joint effort of different groups from public and private research initiatives made it possible to assemble the first domestic sunflower reference genome (draft version 0.2). Its reassessment by blast searches showed the existence of three additional MT coding sequences in the sunflower genome: new MT1 (HaMT1-3), MT2 (HaMT2-4) and MT4 (HaMT4-2) isoforms (Fig. 1). It is important to mention that while the chromosomal location of six out of the ten *HaMT* genes has been verified, it was not possible to allocate a genomic reference position for *HaMT1-1*, *HaMT1-2*, *HaMT4-1* and *HaMT4-2*, as these sequences are still included in scaffolds of the draft assembly. The analysis of the sunflower genome sequences also revealed that most of the *MT* genes are composed of three exons and two introns — *HaMT2-4*, *HaMT4-1* and *HaMT4-2* being exceptions, with two exons and one intron. This is curious, because the 3 exons–2 introns gene structure corresponds to the least frequent among plant *MT* genes, with only type 3 MT genes exhibiting it [6,37]. In conclusion, our reappraisal of the sunflower MT family shows that it is composed of ten isoforms, three belonging to plant MT subfamily 1, four belonging to plant subfamily 2, and only one and two to plant MT subfamilies 3 and 4, respectively.

3.2. Sunflower metallothionein gene expression

In order to evaluate the functionality of the sunflower *MT* genes, expression of each *HaMT* member reported in the NCBI databank was evaluated by quantitative real time PCR with Universal Library Probes (Roche), in roots, leaves and seeds – 21 days postanthesis – of plants grown in a greenhouse for 90 days (Table 1). Unfortunately, this analysis was performed before the release of the sunflower genome draft assembly, this being the reason why data on the expression of the three newly identified genes are not included.

The expression patterns of *HaMT1-2*, *HaMT2-1* and *HaMT2-2* are coincident with those described in the literature for their respective plant MT subfamilies (Fig. 2) [6]. Hence, subfamily 1 plant MTs are the main isoforms in roots, whereas subfamily 2 plant *MT* genes are the most expressed in leaves. However, it is worth noting that these isogenes were found highly expressed in seeds, particularly *HaMT1-2* and *HaMT2-1* (Fig. 2), contrarily to the results found for other plants [14]. *HaMT2-3* expression was not detected in roots, and in leaves it was lower than that of the other *MT2* genes. Curiously, its higher expression level was detected in seeds. Although the expression pattern of *HaMT3* corresponds to the typical profile found for subfamily 3 MTs – higher in leaves, lower in roots – it was never detected in seeds, and its expression levels were very low, respectively 2 and 4 orders of magnitude below that of actin in leaves and roots (Fig. 2). Expression of *HaMT1-1* and *HaMT4-1* was not detected in any of the tissues studied. All these results were compared with transcriptomic data retrieved from the Heliagene portal (Figs. S1–S9) [38], with some similarities – like the expression pattern of *HaMT2-3*, being higher in seeds – and the peculiarity that many *MT* genes are mostly expressed in stems or floral tissues. These data also confirm that sunflower *MT* genes are expressed at very high basal levels in plant tissues, at least in terms of transcript abundance.

Fig. 1. Protein sequence for all the members identified in the sunflower MT family. Each MT is named with the corresponding subfamily number. The shaded boxes indicate the cysteine residues, and histidines are shown in bold. The isoforms marked with an asterisk are those newly identified after the analysis of the sunflower genome draft assembly.

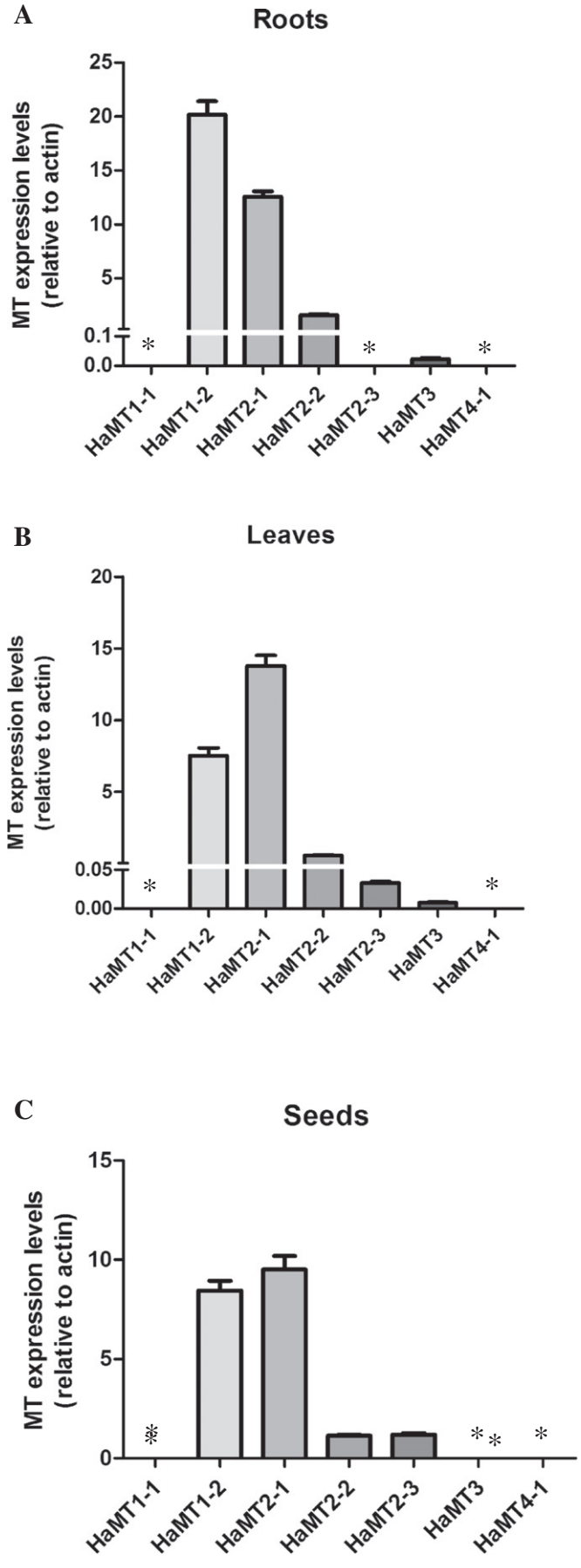

3.3. S. cerevisiae metal tolerance rendered by sunflower MTs

To analyse whether the heterologous expression of sunflower *MT* genes rendered to yeast cells some advantage related to metal tolerance, a resistance experiment was performed using a yeast strain devoid of its two MTs (CUP1 and CRS5), in order to rule out any possible direct or indirect interference by the endogenous peptides. To this end, the cDNAs encoding the most highly expressed sunflower *MT* gene from each subfamily, *CUP1* – the Cu-thionein from *S. cerevisiae* – or *mMT1* – a mammalian (mouse) typical Zn-thionein – were sub-cloned in the multicopy plasmid p424. Subsequently, the *MT*-devoid yeast strain 51-2c-Δc5 was transformed with either one of these constructs or with the non-recombinant p424 as a control. The ability of these transformants to grow in different media supplemented with copper, zinc or cadmium was tested by standard dot assays. The corresponding results (Fig. 3A) clearly show that all sunflower MTs tested are able to restore copper tolerance as efficiently as the yeast copper thionein CUP1, since colony growth was impaired beyond the first dilution for the control cells, while those overexpressing *CUP1* or any *HaMT* yielded colonies even at the fourth dilution range. Noteworthy, the mouse MT1-overexpressing transformants yielded colonies only up to the second dilution range in the 150 μM Cu media tested, this being consistent with the Zn-thionein character of mMT1 [29]. Results are less conclusive as regards divalent metal binding tolerance. Only HaMT3 and HaMT4-1 are able to confer some degree of resistance to zinc, growing up to the fourth dilution, while all the other transformants and the control strain grow up to the third or fourth dilution, but yielding less vigorous colonies. Thus, it should be assumed that only these two MTs confer better Zn-tolerance to yeast cells than the mammalian mMT1. Conversely, when yeast cells are confronted with high cadmium concentrations, growth is seriously hampered, as control cells do not grow at any dilution. In these conditions, most MTs confer only marginal resistance, except for CUP1 and HaMT4-1, which efficiently restore growth. Finally, in order to reassess the Zn resistance conferred by HaMTs, the Zn-sensitive yeast strain (CM104), defective for the Zrc1 and the Cot1 vacuolar zinc transporters, was transformed with all the p424 plasmid constructs (Fig. 3B). In this genetic background all HaMTs performed similarly to the Zn-thionein mMT1, providing a marginal resistance to the metal, as they only grow one dilution more than the control strain transformed with the void p424 vector. In summary, all HaMTs appear to be as good as the yeast Cu-thionein CUP1 in restoring growth at high copper concentrations, but they only confer a marginal resistance in high concentration zinc media. HaMT4-1 seems to be particularly efficient at recovering cadmium resistance, while the other HaMTs perform more modestly.

3.4. Sequence analysis of HaMT1 and HaMT2

As was mentioned above, sunflower MT3 and MT4-1 were recently analysed due to their interest as His-containing peptides [36], but the characterisation of sunflower MT1s and MT2s was still missing. Hence, while the HaMT1-3 sequence shows the 6 + 6 Cys pattern expected for a MT1 protein in its Cys-rich domains, the HaMT1-1 and HaMT1-2 peptides, exceptionally, encompass seven and eight Cys residues, respectively, at their N-terminal Cys-rich domain (Figs. 1 and 4A) [39]. Variants with an additional Cys residue located before the first conserved CXCG motif, as is the case in HaMT1-2 (position 3), are known for several plant MT1s (Table S1). Contrarily, the extra Cys at the end of the N-terminal domain is exclusive to the sunflower HaMT1-1 and HaMT1-2 MTs. The presence of two additional Cys residues in MT1

Fig. 2. Real time PCR analysis of sunflower *MT* gene expression in (A) roots, (B) leaves and (C) seeds of mature plants. The means were generated from three independent measurements, and the bars indicate standard deviations. Asterisks mean that we could not detect expression of the *MT* in the corresponding tissue (see the Experimental section for the developmental stage in which samples were taken).

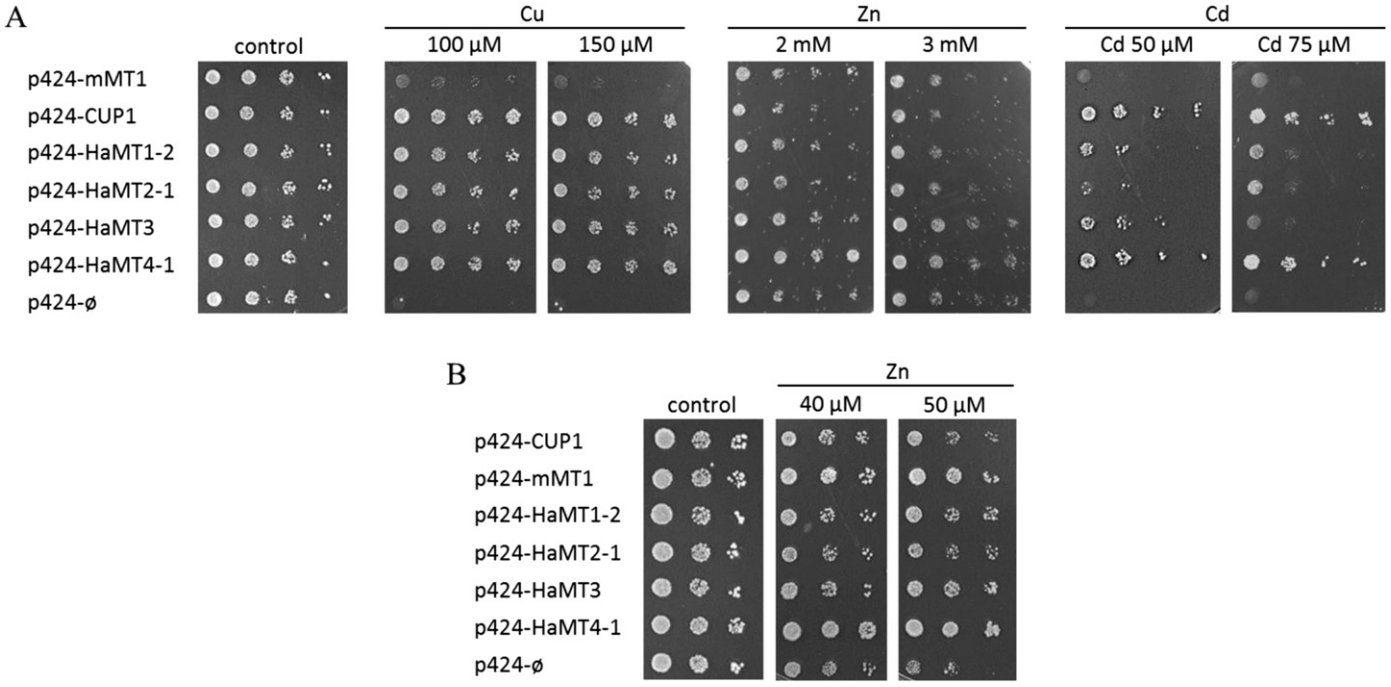

Fig. 3. Effect of the heterologous expression of sunflower *MT* genes (one member of each subfamily of plant MT) in *S. cerevisiae* cells grown under metal stress. (A) 51-2c-Δc5 (*MT null*: *Cu/Cd sensitive*) and (B) CM104 (*zinc sensitive*) cells transformed with the constitutive expression vectors void p424 (control) or the indicated constructions of an MT coding region cloned in p424, and grown in SC agar plates supplemented with the indicated metals. mMT1: mouse metallothionein 1 (canonical Zn-thionein); CUP1: yeast metallothionein (canonical Cu-thionein).

has only been observed for HaMT1-2 and *Huperzia serrata* MT1 (GenBank GO912370; Table S1), but in this latter case they are distributed one in each Cys-rich domain.

The four sunflower peptides classified as plant MT2s (HaMT2-1, HaMT2-2, HaMT2-3 and HaMT2-4, Figs. 1 and 4B) show the CC motif characteristic of this subfamily at the beginning of the N-terminal Cys-rich domain, and all HaMT2 isoforms, except that of HaMT2-4, present the CCXGXCXC and CXCXXXCXGC motifs at the N-terminal domain and the GVAP tetrapeptide conserved within the spacer region [15]. Although MT2s typically exhibit eight and six Cys respectively at their N- and C-terminal domains [6], HaMT2-1 and HaMT2-4 exhibit some changes in relation to this canonical pattern. Thus, HaMT2-1 possesses a seventh Cys at the C-terminal Cys-rich region, analogously to *Fragaria ananassa* and *Ginkgo biloba* MT2 isoforms, also showing one extra Cys at the beginning of their C-terminal domain, although not in the same positions (Table S2). Additionally, there are other variants of plant MT2s showing two or three additional Cys in this region (Table S2). On the other hand, HaMT2-4 shows only seven Cys at its N-terminal region, and unprecedentedly features an additional CC motif at the linker region, followed by another potentially coordinating residue (His). Overall, HaMT1-1, HaMT1-2, HaMT2-1 and HaMT2-4 sunflower MTs feature variations in the number of Cys residues when compared to

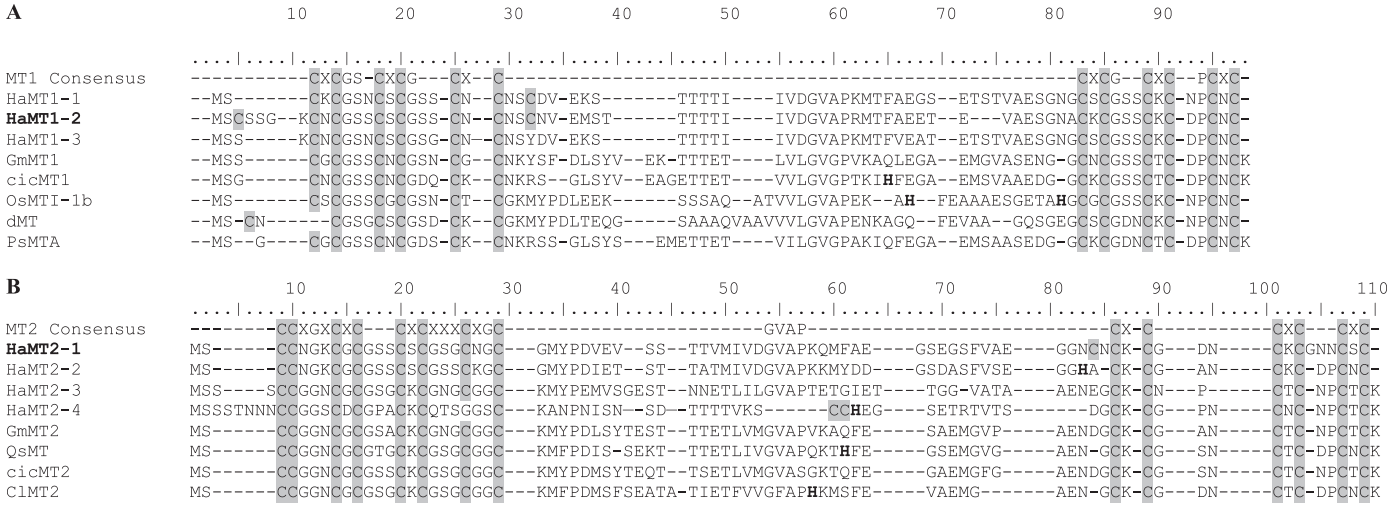

Fig. 4. Amino acid sequences of the sunflower (A) HaMT1 and (B) HaMT2 isoforms. For comparative purposes, the sequences of *G. max* GmMT1 (BQ742738), *C. arietinum* cicMT1 (Q39458), *O. sativa* OsMTI-1b (BAG87041), *T. durum* dMT (AAT99566), *P. sativum* PsMTA (P20830), *G. max* GmMT2 (BQ629803), *Q. suber* QsMT (Q93X22), *C. arietinum* cicMT2 (Q39459) and *C. lanatus* ClMT2 (Q6I674), for which their divalent metal-ion binding abilities have been reported, are included. The shaded boxes indicate the cysteine residues, and histidines are shown in bold. The conserved motifs important for the classification of the peptides into the MT1 (MT1 Consensus) or MT2 (MT2 Consensus) plant MT subfamilies are also shown, where X represents any other amino acid. The MTs analysed in this work (HaMT1-2 and HaMT2-1) are shown in bold.

the canonical plant MT1 and MT2 subfamilies, which may affect their metal-binding properties. None of the MT1s and MT2s for which the metal-binding abilities are known, up to date, shows such extra Cys.

3.5. HaMT recombinant polypeptides: cloning, synthesis and purity

HaMT1-2 and *HaMT2-1* were the HaMT retrieved isoforms that showed a higher copy number of ESTs in the databank, which was indicative of a higher expression level. This was coincident with our qPCR analysis, which pointed to these *MT* genes as the most highly expressed in all the sunflower tissues examined (Fig. 2). Consequently, these two isoforms were selected to study the metal-binding abilities of their encoded peptides. DNA sequencing confirmed that the recombinant plasmids pGEX–HaMT1-2 and pGEX–HaMT2-1 included the expected cDNAs and that these were cloned in the correct frame after the GST coding portion. As a consequence of the GST-fusion construct, the HaMT1-2 and HaMT2-1 peptides heterologously synthesised in this work – from now on named as HaMT1 and HaMT2, respectively – presented the addition of the initial Gly–Ser dipeptide. After corroborating the synthesis of the GST-fused polypeptides in small-scale (3 mL) cultures, the Zn(II)- and Cd(II)–HaMT1 and HaMT2 complexes were obtained from large-scale, metal-enriched cultures (5 L) of the recombinant bacteria. In the final purification step, Zn–HaMT1 eluted from the FPLC column in two overlapping peaks, and thus two fraction pools were separated, one comprising of from 10.0 mL to 11.0 mL (peak 1) and the other from 11.0 mL to 13.5 mL (peak 2) of the eluted volume (Fig. 5A). The content of both peaks was analysed by ESI-MS at pH 2.4 to determine the molecular mass of the apo-peptides present in the sample. Peak 1 uniquely showed a protein of the molecular mass theoretically calculated for HaMT1 (7531.4 Da, Fig. 6A), while in peak 2 this protein was mixed with two additional peptides of 3017.0 ± 0.9 Da and 4529.2 ± 0.6 Da (Fig. 6B). Contrarily, Cd–HaMT1 eluted from the FPLC column rendered a unique peak in the 10.5–13.0 mL range of the elution volume (Fig. 5B). However, the acid ESI-MS analysis of this peak also revealed the presence of a mixture of apo–HaMT1, with the two additional peptides detected in the peak 2 sample of Zn–HaMT1 (Fig. 6C). These two peptides could be unambiguously assigned to the products of the proteolytic HaMT1 cleavage between the Met31 and Ser32 residues, which would give rise to fragments of 3018.3 Da and 4533.1 Da, respectively. Analysis by SDS-PAGE of the total protein extract after IPTG induction (data not shown) as well as the presence of the apo–(Ser^{32}–Cys^{75}) peptide at the end of the purification process, allowed concluding that the cleavage took place after the batch-affinity chromatography due to an auto-proteolysis process. In addition, it is worth noting that cleavage at the linker region has also been reported for other recombinantly synthesised plant MT1s, namely the Cd–MT complexes of *P. sativum* [10] and *T. durum* [40]. Even also auto-proteolytic cleavage has been reported for certain animal MTs, such as the case of recombinant sea urchin MT [41], or the native Cd–MT forms isolated from the earthworm *Eisenia foetida* [42] and the insect *Orchesella cincta* [43]. Conversely, the Zn(II)- and Cd(II)–HaMT2 preparations eluted in one main peak (Fig. 5A and B, respectively). Fractions corresponding to the elution volumes from 9.5 mL to 13.0 mL for Zn–HaMT2, and from 10.5 mL to 12.5 mL for Cd–HaMT2 were recovered, from which a single apo–HaMT2 species was invariably detected, exhibiting the expected molecular mass (7952.9 Da, Fig. 6D), and therefore no proteolytic cleavage have to be assumed for this isoform.

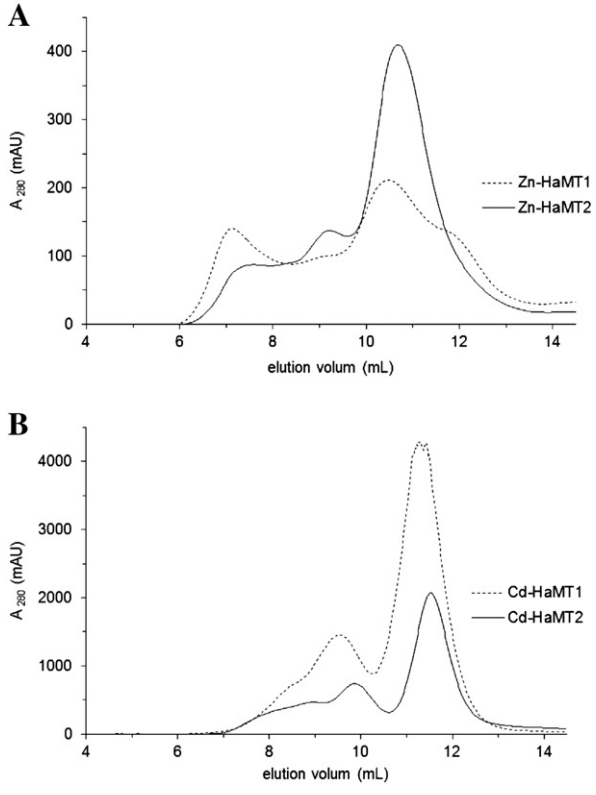

Fig. 5. Elution profile from the Superdex 75 size exclusion FPLC column (equilibrated with 50 mM Tris–HCl, pH 7.0) of the HaMT preparations after thrombin cleavage of the purified GST–HaMT fusion peptides recombinantly synthesised in (A) Zn(II)- and (B) Cd(II)-enriched *E. coli* cultures.

3.6. Characterisation of the M(II)–HaMT1 and HaMT2 recombinant complexes

The characterisation of the Zn(II)–HaMT1 complexes was performed using the peak 1 preparation, which was devoid of cleaved peptides. A mean value of 4.3 Zn(II) ions per MT was revealed by acid ICP-AES (Table 2), which correlated well with the detection of major Zn_3-, Zn_4- and Zn_5–HaMT1 species by ESI-MS (Table 2, Fig. 7A). Interestingly, the ESI-MS spectra at pH 7.0 of the peak 2 of the Zn–HaMT1 preparation revealed that the two proteolytic fragments yielded major Zn_1–(Gly–Met^{31}), Zn_2–(Ser^{32}–Cys^{75}) and minor Zn_3–(Ser^{32}–Cys^{75}) species (Fig. S10). Therefore, since the summation of the Zn(II) content of both moieties never achieves the Zn_5–HaMT1 stoichiometry found for the full peptide, only the assumption of a single cluster involving both the N- and C-terminal Cys-rich domains could account for this complex. However, the Zn_3–HaMT1 and Zn_4–HaMT1 species are compatible with independent Cys-rich Zn-binding domains, although the latter, to a lesser extent, is due to the minor presence of the Zn_3–(Ser^{32}–Cys^{75}) complex. When considering Zn–HaMT2, a 4.4 Zn/MT ratio was determined, which correlated well with the mixture of Zn_4- and Zn_5–HaMT2 species, together with the minor Zn_3–HaMT2 complex detected by ESI-MS (Table 2, Fig. 7B). The CD spectra of both Zn–MT preparations showed a low chirality profile (Fig. 8A), lacking the exciton coupling band centred at *ca.* 240 nm typical of conventional Zn–MTs [33].

Synthesis of HaMT1 in Cd(II)-enriched cultures yielded an average 6.1 Cd/HaMT1 ratio, as determined by acid ICP-AES (Table 2), while the differences observed between the conventional and acid ICP-AES measurements suggested the presence of acid-labile sulphide ligands [35]. Indeed, ESI-MS analyses revealed the presence of major Cd_6S_8- and Cd_7S_7–HaMT1 species as well as minor Cd_7S_1- and Cd_7S_3–HaMT1 complexes (Table 2, Fig. 7C). For Cd–HaMT2, the ICP-AES analyses of the recombinantly synthesised Cd(II)–HaMT2 revealed a mean 6.3 Cd/MT content (Table 1), which is in agreement with the major Cd_6S_8–HaMT2 and minor Cd_6–HaMT2 species detected by ESI-MS (Table 2, Fig. 7D). Although the differences between conventional and acid ICP-AES data did not support the existence of sulphide ligands

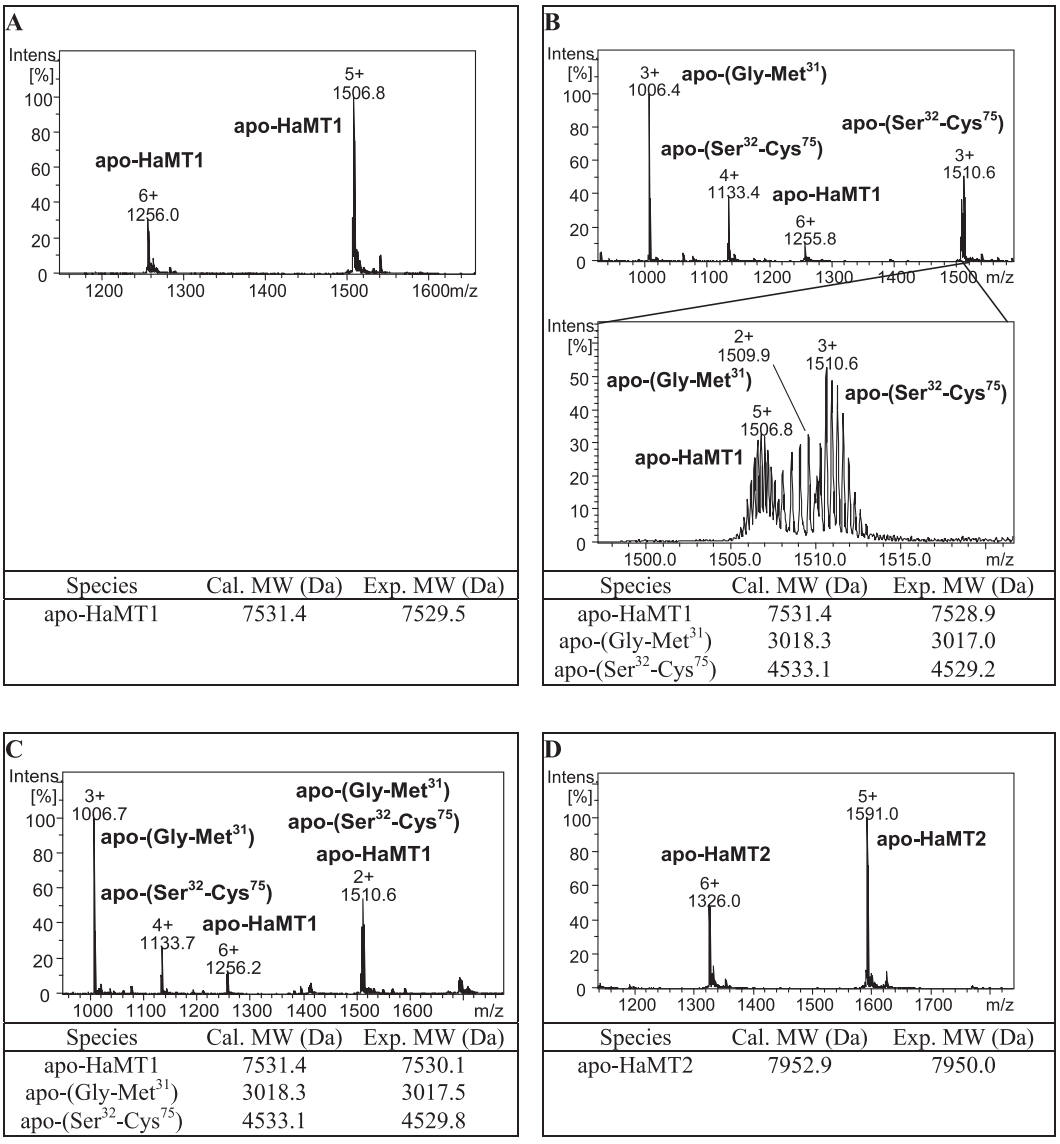

Fig. 6. ESI-MS spectra recorded at pH 2.4 of (A) Zn–HaMT1 peak 1, (B) Zn–HaMT1 peak 2, (C) Cd–HaMT1 and (D) Zn–HaMT2 and Cd–HaMT2. A zoomed view from the 1497 to 1522 m/z spectrum region is shown in (B). The error associated with the experimental MW values was always lower than 0.1%. Cal. MW: calculated (or theoretical) molecular weight; ad Exp. MW: experimental molecular weight.

in this case, the intense absorptions at the 270–290 nm range (data not shown) confirmed their presence [35]. Moreover, the CD spectra of both Cd–HaMT1 and Cd–HaMT2 preparations exhibited complex profiles with important contributions at the low energy wavelength region (Fig. 8B), this providing a further confirmation of the participation of sulphide ligands into the Cd–HaMT complexes. In fact, they are very close to what we attributed to type C fingerprints [35], like those shown by the Cd–MTN complexes of one of the Cu-thionins of *Drosophila*, which feature an exciton coupling at *ca.* 250 nm and an intense Gaussian band at *ca.* 280 nm.

Table 2
Analytical characterisation of the recombinant HaMT1 and HaMT2 preparations synthesised in Zn(II)- and Cd(II)-enriched media.

Protein	Zn–MT complexes			Cd–MT complexes		
	Protein concentration[a] ($\times 10^{-4}$ M)	Zn/MT content[b]	Zn–MT species[c]	Protein concentration[a] ($\times 10^{-4}$ M)	Cd/MT content[b]	Cd–MT species[c]
HaMT1	1.3/1.3	4.6/4.3	**Zn_4, Zn_3, Zn_5**	1.1/0.8	5.0/6.1	**Cd_6S_8, Cd_7S_7** Cd_7S_3, Cd_7S_1
HaMT2	1.0/0.8	4.5/4.4	**Zn_4, Zn_5** Zn_3	0.4/0.4	6.8/6.3	**Cd_6S_8** Cd_6

[a] Protein concentration calculated from the sulphur content measured by normal and acid ICP-AES, respectively.
[b] Metal per MT molar ratio calculated from the total metal and sulphur content measured by normal and acid ICP-AES, respectively. Both Zn and Cd levels were quantified in all samples, but only the metals present at detectable amounts are indicated. In the case of Zn–HaMT1, only the values recorded from peak 1 are shown.
[c] Metal/MT molar ratio calculated from the difference between holo- and apo–protein molecular masses obtained from ESI-MS. Species shown in bold correspond to the major species in the preparations.

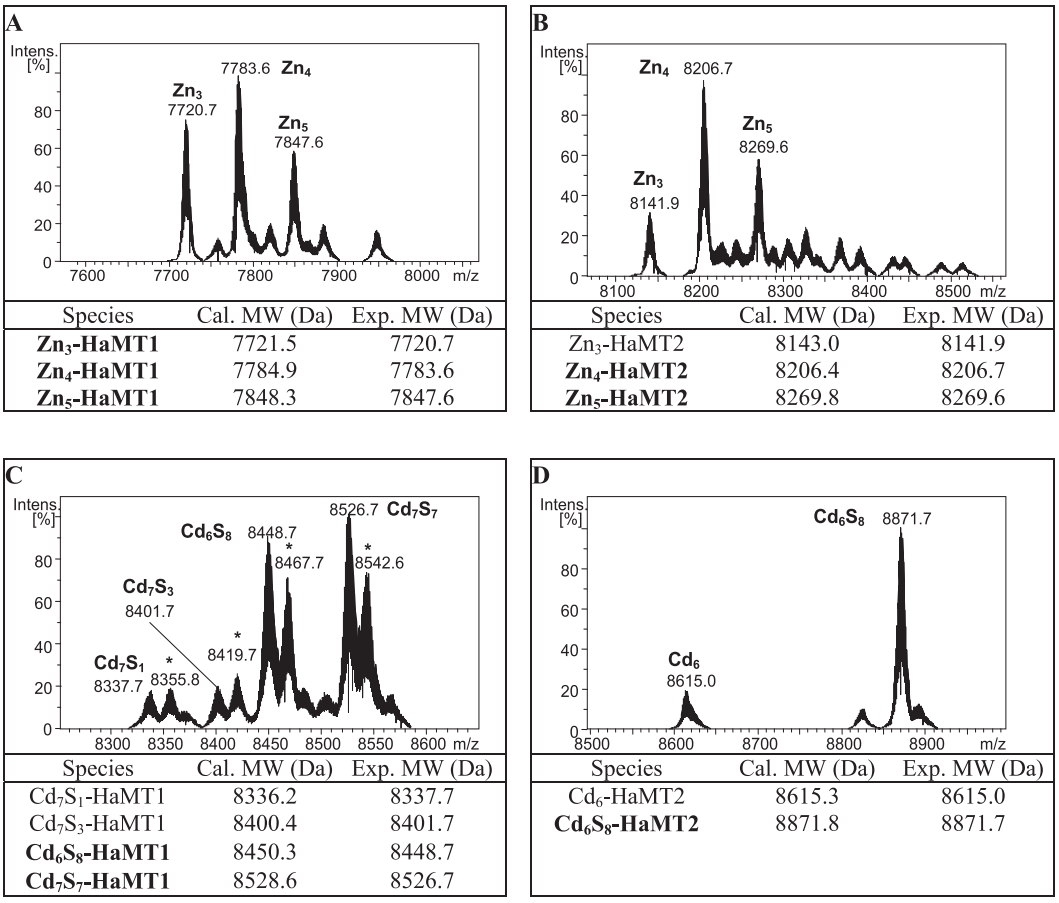

Species	Cal. MW (Da)	Exp. MW (Da)
Zn_3-HaMT1	7721.5	7720.7
Zn_4-HaMT1	7784.9	7783.6
Zn_5-HaMT1	7848.3	7847.6

Species	Cal. MW (Da)	Exp. MW (Da)
Zn_3-HaMT2	8143.0	8141.9
Zn_4-HaMT2	8206.4	8206.7
Zn_5-HaMT2	8269.8	8269.6

Species	Cal. MW (Da)	Exp. MW (Da)
Cd_7S_1-HaMT1	8336.2	8337.7
Cd_7S_3-HaMT1	8400.4	8401.7
Cd_6S_8-HaMT1	8450.3	8448.7
Cd_7S_7-HaMT1	8528.6	8526.7

Species	Cal. MW (Da)	Exp. MW (Da)
Cd_6-HaMT2	8615.3	8615.0
Cd_6S_8-HaMT2	8871.8	8871.7

Fig. 7. Deconvoluted ESI-MS spectra recorded at pH 7.0 for (A) Zn–HaMT1 peak 1, (B) Zn–HaMT2, (C) Cd–HaMT1 and (D) Cd–HaMT2. Species shown in bold correspond to the major species present in the preparations. The asterisk (*) indicates ammonia adducts (+18 Da) of the corresponding metallospecies shown on the left. The error associated with the experimental MW values was always lower than 0.1%. Cal. MW: calculated (or theoretical) molecular weight; and Exp. MW: experimental molecular weight.

3.7. Zn(II) with Cd(II) replacement studies and acidification–reneutralisation experiments of the Cd(II)–HaMT1 and Cd(II)–HaMT2 biosynthesised complexes

Further information about the Cd(II)-binding properties of HaMT1 and HaMT2 was obtained from the analysis of the Zn/Cd replacement on Zn(II)-loaded MTs, as well as from the acidification plus subsequent reneutralisation of the recombinant Cd(II)–MT complexes.

The UV data recorded during the successive addition of Cd(II) to Zn–HaMT1 showed a gradual incorporation of Cd(II) to HaMT1 up to the fifth Cd(II) eq added, since the absorptions at *ca.* 250 nm, typical of Cd–(SCys) chromophores, developed during this stage (Fig. 9A–B). But it was not until the addition of the fifth Cd(II) eq that the initial, and until now almost invariant CD spectrum, started to develop the absorptions observed for the biosynthesised Cd–HaMT1 sample (Figs. 9C and 10A). Thereafter, the CD spectra evolve through an isodichroic point at *ca.* 250 nm to finally reach its maximum intensity after 7 Cd(II) eq added. At this point the CD envelope resembles that of the recombinant Cd–HaMT1, although with a significantly lower chirality (Fig. 10A), thus suggesting the existence of a similar fold but a more flexible and/or less compact Cd–thiolate cluster for the in vitro formed species. ESI-MS measurements of aliquots extracted at different stages indicated the presence of major Cd_5–HaMT1 and Cd_6–HaMT1 species in solution, together with a minor Cd_4–HaMT1 form (Fig. S11). No significant spectroscopic or spectrometric differences were observed after the addition of further Cd(II) ions (Figs. 9, S11), but significantly the addition of 1 and 2 S^{2-} eq caused an increase in the intensity of the 280(+) nm CD absorption band (Fig. 9C), leading to a CD fingerprint with a closer resemblance to that of recombinant Cd–HaMT1, although again with much less intensity (Fig. 10A). Similar results were obtained after acidification–reneutralisation of the biosynthesised Cd–HaMT1 complex, followed by the addition of up to 6 S^{2-} eq (Fig. 10A). Thus, the data fully confirm the significant presence of sulphide ligands in the biosynthesised Cd–HaMT1 preparations, and indicate that Cd_4-, Cd_5- and Cd_6–HaMT1 are the most favoured species when Zn(II) is replaced by Cd(II) in HaMT1. Moreover, the data also suggest the presence of small S^{2-} amounts in the biosynthesised Zn–HaMT1 sample, since during the addition of 5 to 9 Cd(II) eq to the protein preparation a positive Gaussian band at *ca.* 280 nm develops without the need of S^{2-} addition (Fig. 9C). In fact, the minor ESI-MS peaks at 7755, 7819 and 7882 Da of the recombinant Zn–HaMT1 preparation (Fig. 7A) corresponds to the Zn_3S_1-, Zn_4S_1- and Zn_5S_1–HaMT1 species, respectively. Unfortunately, and probably because of the low amount of these acid labile sulphide ligands, no variations were detected between conventional acid ICP-AES (Table 2).

An analogous treatment of Zn–HaMT2 with Cd(II) rendered similar results to those of Zn–HaMT1, with UV spectra showing that binding of Cd(II) occurs up to the sixth Cd(II) eq added (Fig. 11A–B). ESI-MS analyses revealed the presence of a major Cd_6–HaMT2 species after the addition of the fifth Cd(II) eq to Zn–HaMT2, while minor Cd_4-, Cd_5-, Cd_5Zn_1- and Cd_7-species were also detected (Fig. S12). From this point onwards, the speciation determined by ESI-MS remained constant, with the only exception of the final disappearance of the Cd_5Zn_1–HaMT2 species (Fig. S12). Thus, these results support the idea that Cd_6–HaMT2 is the main species present when Zn(II) is replaced by Cd(II) in the Zn–HaMT2 preparation. The evolution of the CD

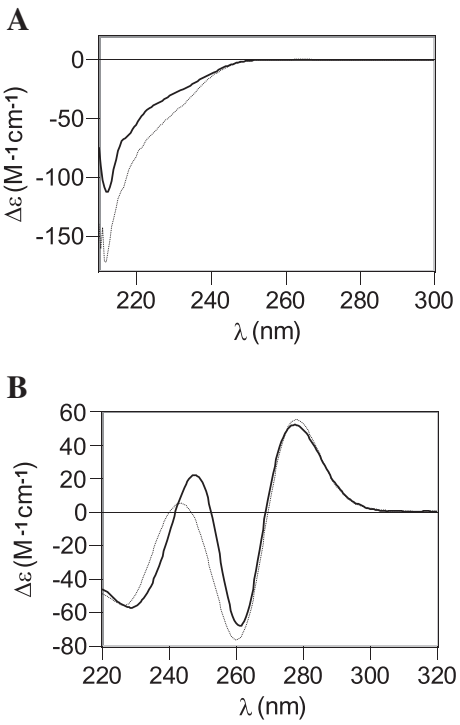

Fig. 8. CD spectra corresponding to the recombinant (A) Zn(II)–HaMT1 (gray dotted line) and HaMT2 (black solid line) complexes, and (B) Cd(II)–HaMT1 (gray dotted line) and HaMT2 (black solid line) complexes.

fingerprints (Fig. 11C) showed that the typical Cd–MT Gaussian band centred at *ca.* 250 nm initially formed at the beginning of the Zn/Cd displacement reaction was progressively converted into a final spectrum through an isodichroic point at *ca.* 255 nm (from 4 to 7 Cd eq), which with the addition of 2 S^{2-} eq resembled the CD fingerprint of recombinant Cd–HaMT2 although with much less intensity (Fig. 10B), analogously to what has been seen for HaMT1. Once more, the addition of S^{2-} ions contributed to reach a CD envelope closer to that of the recombinant preparations, thus confirming the presence of such ligands in Cd–HaMT2, and probably also in Zn–HaMT2 but to a much lesser extent (minor peaks at 8304 and 8367 Da in Fig. 7B are attributable to Zn_5S_1- and Zn_6S_1–HaMT2, respectively). Concordantly, a weaker but similar CD profile to that of recombinant Cd–HaMT2 was obtained after an acidification–reneutralisation process plus the addition of 5 S^{2-} eq to the biosynthesised Cd–HaMT2 preparation (Fig. 10B).

4. Discussion

The results presented here report eight novel plant MT isoforms encoded in the sunflower (*H. annuus*) genome, in addition to the two isoforms already described and analysed [36]. The analysis of the expression profile of seven of these *MT* genes shows that many of them are transcribed at very high basal levels, particularly *HaMT1-2* and *HaMT2-1* (Fig. 2), while we could not detect any expression of *HaMT1-1* and *HaMT4-1*. The negative results for subfamily MT4 are explainable because their mRNAs are restricted only to seeds, and possibly gene expression was not turned on at the developmental stage of the seeds analysed in this work (21 days post-anthesis). Seed development in *A. thaliana* takes 19 days [44], and plant *MT4* (*MT4a*/*MT4b*) expression turns on between 7 and 8 days after pollination [45], coinciding with the onset of storage reserve accumulation. In contrast, seed development in sunflower takes approximately 70 days, and reserve accumulation exponential increase takes place after 30 days post-anthesis in sunflower [46]. However, our data resulted highly unusual for subfamily MT1. We have only examined expression in root, leaf and seed tissues, but data from HeliaGene transcriptomics [38] show that most sunflower *MTs* are highly expressed in stems and/or flower structures (Figs. S1–S9), pointing towards a potential role in metal transport from roots to shoots and/or to seeds. The heterologous expression of the most highly expressed isogenes of each type of HaMT in different yeast strains sensitive to metals show that all of them can restore copper tolerance, but none of them is very efficient at re-establishing zinc tolerance, with HaMT3 and HaMT4-1 being slightly better at this function. As regards cadmium detoxification, HaMT4 is by far the most effective sunflower MT, this confirming that HaMT4, like most plant MT4 peptides [14,47,48], are better adapted to handle divalent metals. Nevertheless these results should be interpreted with care, as they only indicate the general abilities of those MTs to bind a specific metal, but it is not a clear or absolute indication of the native, in planta, function [9].

Analysis of the protein sequence of the HaMT isoforms reveals that two of the peptides belonging to the MT1 subfamily do not feature the canonical subfamily Cys content, since they present fourteen and fifteen Cys instead of twelve (Fig. 1). Two out of the four MT2 polypeptides contain the standard fourteen Cys in the MT2 subfamily, while the other two present either one additional Cys at the C-terminal Cys-rich region or an additional CC motif in the centre of the spacer (Fig. 1). Therefore, they were an extremely suitable material to characterise the effect of Cys variability in plant MT metal-binding abilities.

The synthesis of HaMT1 in Zn(II)-enriched media mainly yielded a mixture of Zn_3-, Zn_4- and Zn_5–HaMT1 complexes (with Zn_4–HaMT1 being the most abundant species), providing an average value of 4.3 Zn/MT. These results are only slightly different from those obtained for other plant MT1 isoforms (Table 3). Hence, in the same conditions, soybean GmMT1, a model of the paradigmatic twelve (6 + 6) Cys pattern of plant MT1s, rendered Zn_4–GmMT1 as the major species, with only a very residual proportion of Zn_3- and Zn_5–GmMT1 complexes [14]. Chickpea cicMT1, containing also twelve Cys plus an additional His residue, showed the Zn_4–MT1 form as almost the unique species detected by ESI-MS, although a fifth Zn(II) ion was hypothesised to be weakly bound, according to spectroscopic data [13]. Thus, it seems reasonable to deduce that the paradigmatic MT1 isoforms yield a canonical Zn_4–MT1 complex, while increasing the number of potential coordinating residues, either Cys (HaMT1) or His (cicMT1) allows a significant presence of Zn_5–MT1, although always coexisting with Zn_4–MT1, which would still remain as the major species. It is also interesting to point out that the Gly–Met^{31} and Ser^{32}–Cys^{75} fragments of HaMT1 only bind 1 Zn(II) and 2–3 Zn(II) ions, respectively, thus suggesting that at least the Zn_5–HaMT1 species would be formed by a single cluster involving both the N- and C-terminal Cys-rich domains. Concordantly, it was also hypothesised that the fifth Zn(II) bound to cicMT1 would only be allocated when the peptide folded into a single Zn_5–$(SCys)_{12}$ cluster, while it could only coordinate 4 Zn(II) ions into two separated Zn_2–$(SCys)_6$ clusters [13]. A single Zn_5–$(SCys)_{14}$ cluster involving both Cys-rich domains was also hypothesised for chickpea Zn_5–cicMT2 [20], containing fourteen Cys. Single joint clusters were also proposed for the Zn_4- and Cu_8-complexes from cork oak MT2, QsMT [32], containing fourteen Cys as well (Table 3). Thus, considering the observed metal-to-ligand stoichiometries (1:2.4 for Zn_5–$(SCys)_{12}$, 1:3 for Zn_2–$(SCys)_6$, and 1:2.8 for Zn_5–$(SCys)_{14}$), it is reasonable to assume the existence of the Zn_1–(Gly–Met^{31}) and the Zn_2–(Ser^{32}–Cys^{75}) species, since a Zn_1–$(SCys)_4$ complex could be formed by the HaMT1 N-terminal moiety (containing eight Cys) and a Zn_2–$(SCys)_6$ cluster could be also envisaged for the C-terminal segment (with six Cys). Therefore, in contrast to the hairpin model proposed for the folding of the Zn_5–HaMT1 species, the detected Zn_3–HaMT1 and Zn_4–HaMT1 species are compatible with a dumbbell model, which accounts for independent Cys-rich Zn-binding domains.

HaMT2 binds a mean value of 4.4 Zn/MT, which corresponds to a mixture of Zn_4- and Zn_5–HaMT2 complexes accompanied by a minor Zn_3 species. Almost the same results were reported for soybean

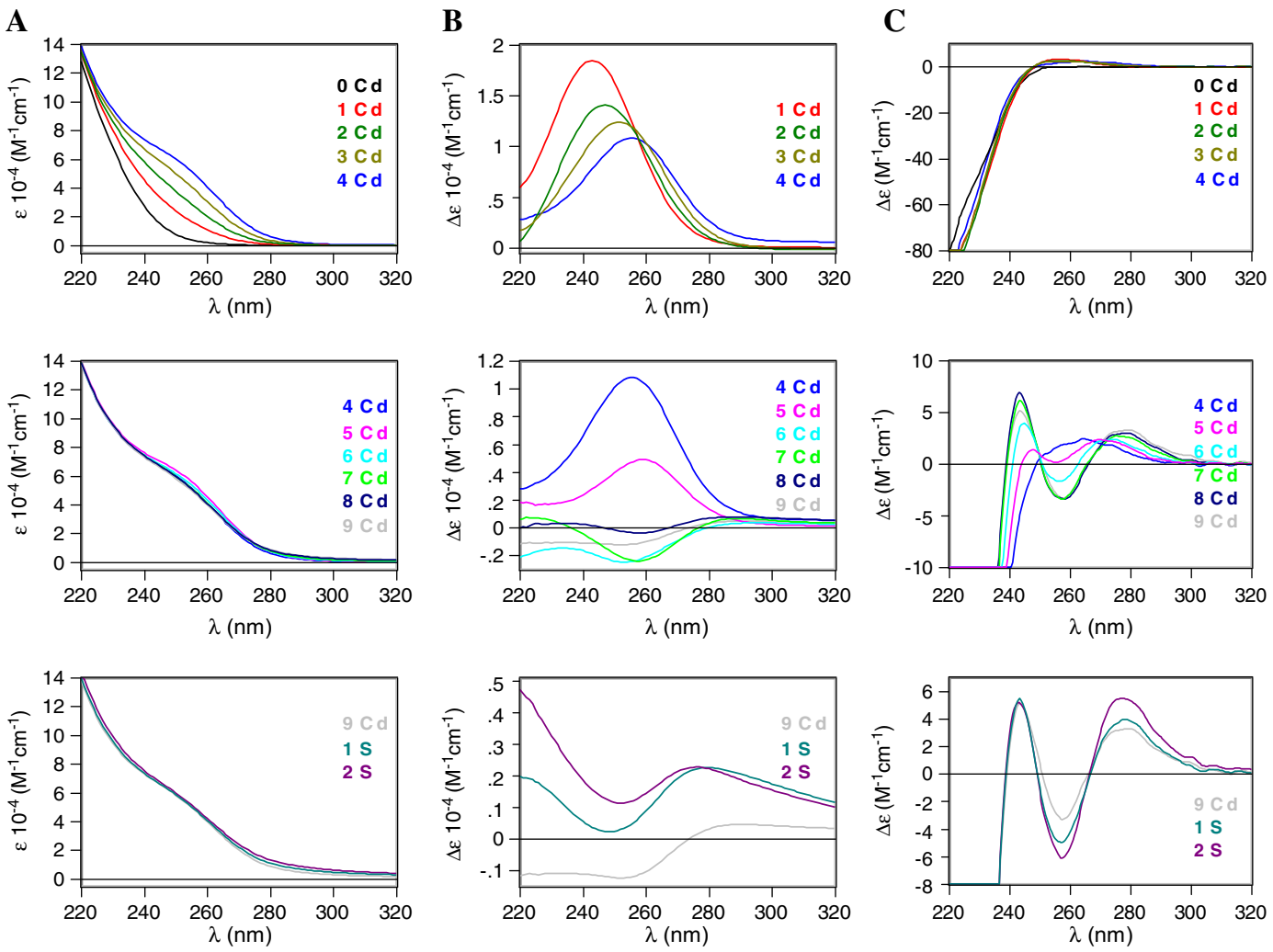

Fig. 9. UV (A), difference UV (B) and CD (C) spectra corresponding to the Cd(II) addition to a 15 μM solution of Zn–HaMT1 peak 1 at pH 7. Each spectrum shown in (B) is the result of the subtraction of the UV spectrum corresponding to the number of Cd(II) equiv shown minus the UV spectrum corresponding to the immediately previous addition.

Zn–GmMT2 [14], which lacks the Cys63 present in HaMT2. Moreover, the same major Zn_4–MT species was detected for cork oak QsMT [18,19], while Zn_5–MT was the major detected species for chickpea cicMT2 [20], although both contain fourteen Cys residues. The Zn/MT molar ratio was 3.6 in the case of watermelon MT2, ClMT2 [17] (Table 3). Thus, the extra Cys present in HaMT2 does not apparently increase its Zn(II)-binding abilities compared to GmMT2, QsMT or cicMT2, whereas data on ClMT2 curiously match those of QsMT, with both peptides containing fourteen Cys and one His residues. Therefore, surprisingly, a poorer mean Zn(II) content is observed for His-containing MT2 isoforms compared to His-devoid MT2s.

Cd(II) coordination studies invariably yielded greater metal ion contents if compared to those of Zn(II) and, as generally observed for Cd(II), the complexity of the final sample was notably increased. Hence, the synthesis of HaMT1 in Cd(II)-enriched cultures yielded sulphide-containing complexes, with Cd_6S_8- and Cd_7S_7–HaMT1 being the major species, and with a concordant mean metal content of 6.1 Cd/MT. These results are in agreement with those corresponding to GmMT1, which yielded a mixture of species where Cd_6S_1–GmMT1 was the major complex, together with Cd_5S_6–GmMT1 in second place [14]. Atomic absorption measurements have revealed a 5 Cd/MT ratio for chickpea cicMT1, and 4(±1) and 4.8 Cd(II) for wheat dMT and rice OsMTI-1b undigested GST-fusion proteins, respectively [11,12]. Therefore, it is clear that the incorporation of acid-labile sulphide ions enhances the Cd-binding capacity of plant MTs, as already demonstrated previously [18,19,49,50]. For Cd–QsMT complexes from cork oak, it was shown that the presence of 2–3 sulphide ions allowed the binding of 1–2 extra Cd(II) ions. Also, the binding of 7 sulphide ions raised the metal content of chickpea cicMT2 from 5 to 9 Cd(II) ions. Therefore, and according to the literature [50], a mean incorporation of 1.5–1.75 S^{2-} per MT would lead to an increase in the binding capacity of these MTs in one additional Cd(II) ion. Remarkably, the Zn/Cd replacement experiments indicated that the maximum loaded Cd-species for HaMT1 is Cd_6, thus becoming the upper limit that cannot be surpassed under these in vitro conditions. However, the constant detection of a mixture of the Cd_4-, Cd_5- and Cd_6–HaMT1 species during the treatment of Zn–HaMT1 with increasing amounts of Cd(II) lead to conclude that there is an equilibrium between the three Cd(II)-loaded species. Hence, the presence of the Cd_4- and Cd_5–HaMT1 species is in agreement with the 4(±1), 4.8 and 5 Cd/MT ratios found for GST–dMT, GST–OsMTI-1b and cicMT1 [11–13], respectively, which contain only twelve Cys residues, while the existence of the Cd_6–HaMT1 species could be only comparable to the 5.8 Cd/MT content found for GST–PsMTA [10], which also contains twelve Cys and for which the presence of sulphide ligands has not been determined (Table 3). Therefore, our results clearly point to an enhanced Cd-binding capacity for HaMT1, probably due to the participation of the extra Cys residues.

Surprisingly, HaMT2 has been shown to render an almost unique Cd_6S_8–HaMT2 complex when synthesised in Cd-enriched cultures, only accompanied by very minor sulphide-devoid Cd_6–HaMT2 species.

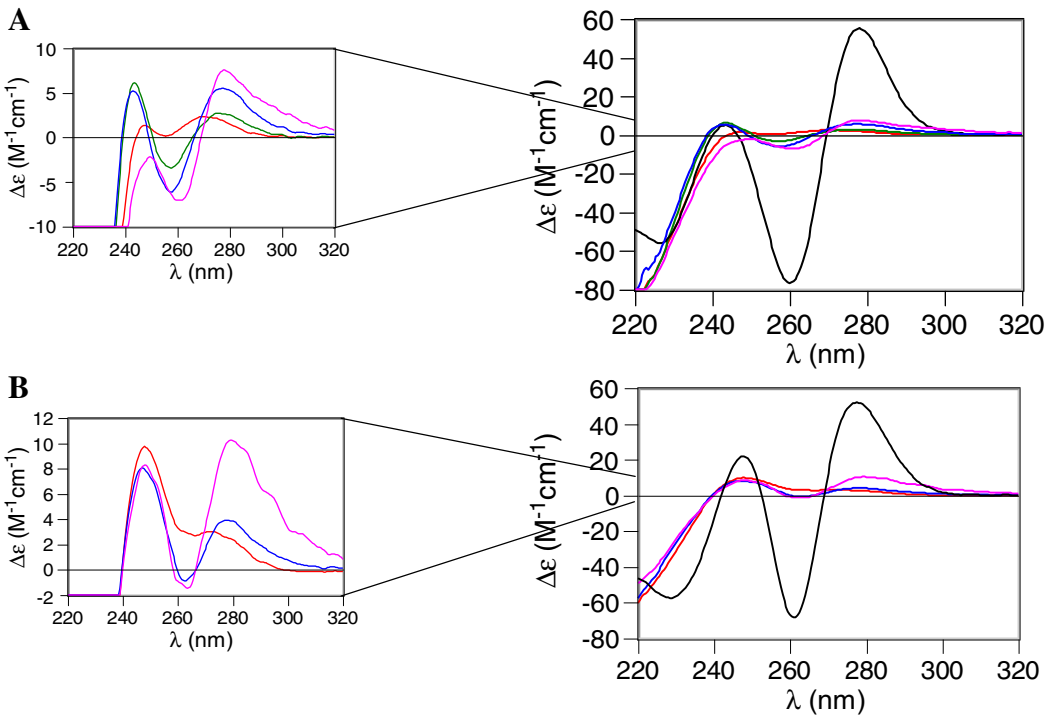

Fig. 10. Comparison of the CD spectra of: (A) the recombinantly synthesised Cd–HaMT1 species (black line), the solution obtained after adding 5 Cd(II) eq (red line), 7 Cd(II) eq (green line) and 9 Cd(II) eq plus 2 S^{2-} eq (blue line) to Zn–HaMT1 (peak 1), and the solution recovered after an acidification–reneutralisation process plus the addition of 6 S^{2-} eq to the recombinant Cd–HaMT1 preparation (pink line); (B) the recombinantly synthesised Cd–HaMT2 species (black line), the solution obtained after adding 6 Cd(II) eq (red line) and 8 Cd(II) eq plus 2 S^{2-} eq (blue line) to Zn–HaMT2, and the solution recovered after an acidification–reneutralisation process plus the addition of 5 S^{2-} eq to the recombinant Cd–HaMT2 preparation (pink line). A zoomed view of each figure has been added for increasing the degree of resolution of the low-intensity CD spectra.

Although the presence of S^{2-} could not be confirmed by the difference between conventional and acid ICP-AES data, it was corroborated by the intense CD absorption that the corresponding preparation exhibited at the 270–290 nm range [35]. Interestingly, the CD fingerprints of Cd–HaMT1 and Cd–HaMT2 were highly similar, with a *ca*. 250 nm exciton coupling band and a Gaussian band centred at *ca*. 280 nm. Moreover, the CD envelope of the reconstituted Cd_9S_7–cicMT2 from chickpea shows completely equivalent signals [49], thus suggesting a similar fold for these three polypeptides. The formation of the Cd_6S_8–HaMT2 complex can be compared to the obtained Cd_6S_1–GmMT2 [14] and Cd_6S_4–QsMT [19] complexes, since these three polypeptides bind 6 Cd(II) ions into sulphide-containing complexes — although the structure of the respective metal cores has necessarily to be distinct given the different Cd:S(Cys):S^{2-} ratios. The main species when Zn is substituted by Cd in Zn–HaMT2 is Cd_6–HaMT2, and 6 Cd(II) is the maximum binding capacity determined for any other plant MT2 isoform under these conditions.

As commented before, transcriptomics data support a potential role for plant MT1s as transporters of metal ions through roots and stems [38 and our data]. This alleged function would rely on a mechanism ensuring a subsequent easy liberation of the metal ions for transfer to the target molecules/structures. Precisely, proteolysis of the metal-MT complexes has been recently claimed as one of these mechanisms [51], and this would be totally coincident with the data here presented, showing the high susceptibility of the HaMT1 complexes to proteolytic cleavage. It is also worth noting that a poor yield for the *G. max* MT1 recombinant synthesis was also reported in our analysis of the *G. max* MT system [14]. Therefore, the structure/function relationships on MTs may obey to two opposite purposes, because metal ion transfer/delivery functionality would be better served by relatively unstable metal-MT species, while a deposit/detoxification aim would better rely on highly stable complexes. These two scenarios, here represented respectively by the HaMT1 and HaMT2 properties, would also resemble the situation found in snail MTs, where the Cu–MT isoform, supposedly involved in Cu handling associated to haemocyanin metabolism, has been shown to form less stable Cu-complexes than a one residue site-directed mutant [29,52], while the detoxifying Cd-thionein forms maximally stable Cd-species [29]. It would be advisable to consider these scenarios when seeking for MT putative roles in organisms, a question far from being conclusively resolved [53].

5. Conclusions

The thorough in silico analysis of the sunflower genome reveals the presence of ten expressed genes, this illustrating the much more pronounced complexity of the plant MT systems in relation to the animal organisms. The sunflower MT peptides belong to the four plant MT subfamilies: three HaMT1, four HaMT2, one HaMT3 and two HaMT4 isoforms. Our mRNA quantification results show that many of the *HaMT* genes are transcribed at a considerable level, concordantly with the data available on transcriptomics databases. However, specific discrepancies between these two sources of information suggest that the conditions/time of collection of the original samples may be determinant when analysing these kinds of results.

The divalent metal ion binding characterisation of HaMT1-2 and HaMT2-1 indicates that in both cases the variation in the number of Cys does not drastically modify their M(II)-binding properties, but instead modulates the degree of heterogeneity of the corresponding recombinant preparations. Overall, comparison of the results for Zn(II)- and Cd(II)-binding properties suggests the hypothesis that the HaMT2 isoforms are probably associated to Cd(II) metabolism and detoxification. In contrast, the MT1 peptides may be associated to functions more related to the transport and delivery of physiological metal ions in plants, as pointed out by their higher presence in roots and stems, and their tendency to proteolytic cleavage.

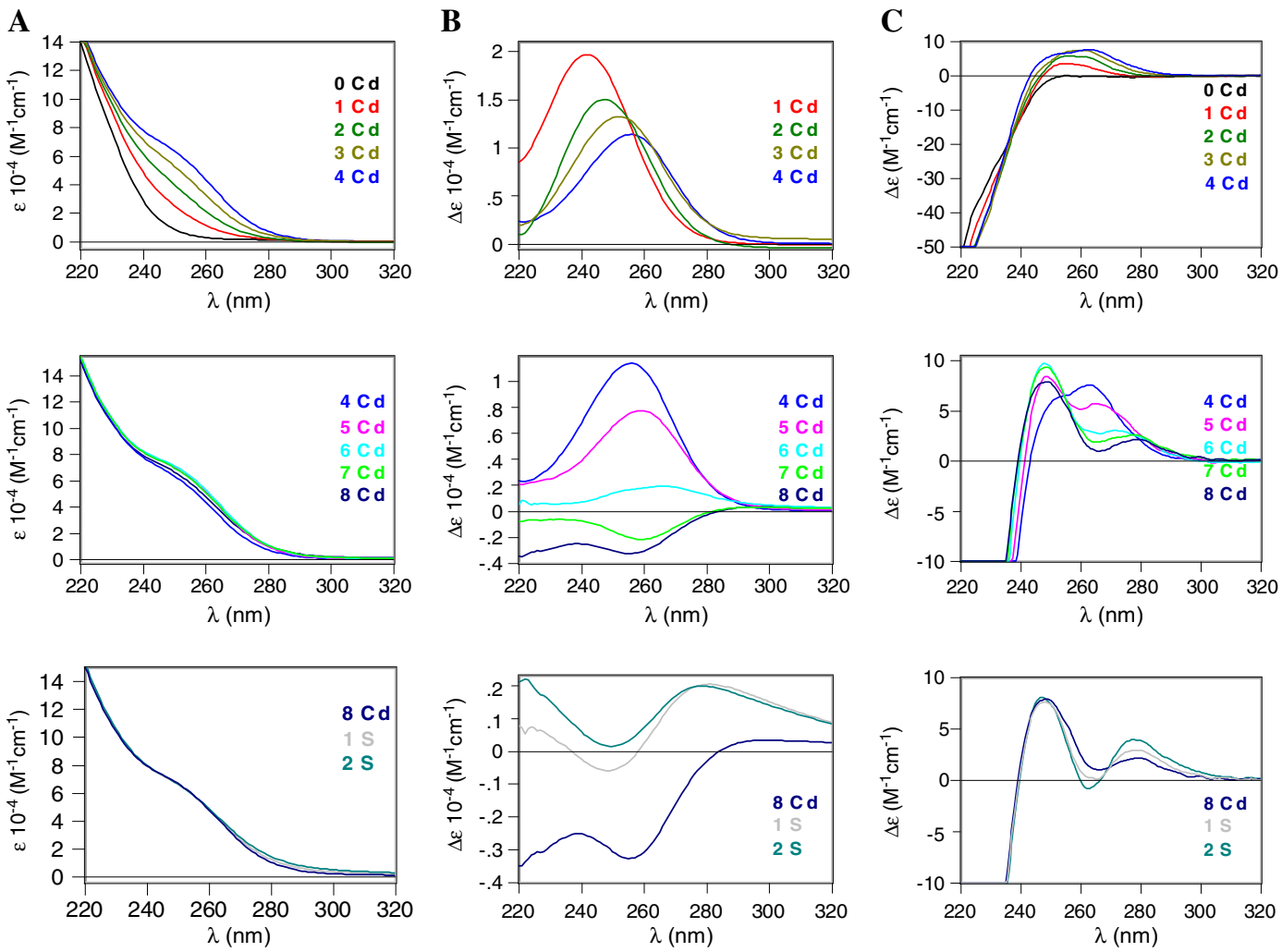

Fig. 11. UV (A), difference UV (B) and CD (C) spectra corresponding to the Cd(II) addition to a 15 μM solution of Zn–HaMT2 at pH 7. Each spectrum shown in (B) is the result of the subtraction of the UV spectrum corresponding to the number of Cd(II) equiv shown minus the UV spectrum corresponding to the immediately previous addition.

Acknowledgements

This work was supported by the Spanish Ministerio de Economía y Competitividad, Grants BIO2012-39682-C02-01 (to SA) and 02 (to MC), which are co-financed by the European Union through the FEDER program, and from CONICET (Argentina) PIP 2011-2013 0061 (to MAP). Authors from both Barcelona universities are members of the 2014SGR-00423 Grup de Recerca de la Generalitat de Catalunya. Cooperation with Argentina was financed by the "Acción Integrada" Grants AR2009-0011 (Spain) and ES09/02 (Argentina). SA was also a recipient of financial help from the Universitat de Barcelona (2014) to promote internationalization. We thank the Centres Científics i Tecnològics

Table 3
Summary of Zn(II)- and Cd(II)-binding properties of plant MT1 and MT2 proteins.

Protein	Cys	His	Zn/MT content[a]	Recombinant Zn–MT species[b]	Cd/MT content[a]	Recombinant Cd_xS_y–MT species[b]	Reconstituted Cd_xS_y–MT species[c]
HaMT1	14 (8 + 6)	0	4.3	Zn_4, Zn_3, Zn_5	6.1	Cd_6S_8, Cd_7S_7	Cd_4, Cd_5, Cd_6
GmMT1	12 (6 + 6)	0	3.8	Zn_4	8.1	Cd_6S_1	–
cicMT1	12 (6 + 6)	1	5	Zn_4	5	–	–
GST–OsMTI-1b	12 (6 + 6)	2	1.8	–	4.8	–	–
GST–PsMTA	12 (6 + 6)	0	–	–	5.8	–	–
GST–dMT	12 (6 + 6)	0	–	–	4 (±1)	–	–
HaMT2	15 (8 + 7)	0	4.4	Zn_4, Zn_5	6.3	Cd_6S_8	Cd_6
GmMT2	14 (8 + 6)	0	4.3	Zn_4, Zn_5	6.7	Cd_6S_1	–
QsMT	14 (8 + 6)	1	3.5	Zn_4	5.3/6.5	Cd_5/Cd_6S_4	Cd_7S_9
cicMT2	14 (8 + 6)	0	5	Zn_5	5	–	Cd_5
ClMT2	14 (8 + 6)	1	3.6	–	–	–	–

[a] Metal per MT molar ratio measured by ICP-AES or F-AAS. The cadmium content for the GST–dMT peptide was exceptionally determined by MALDI-TOF-MS.
[b] Major Zn(II)–MT species detected by ESI-MS in the recombinantly obtained preparations.
[c] Major Cd(II)–MT species detected by ESI-MS in the solutions obtained either after Zn/Cd replacement plus S^{2-} addition to Zn–MT (HaMT1, HaMT2, QsMT) or after reconstitution of apo–MT with Cd(II) (cicMT2). The data for HaMT1 and HaMT2 (in bold) are from this work, and the data for other MTs are from the literature: GmMT1 and GmMT2 [14], cicMT1 [13], GST–OsMTI-1b [12], GST–PsMTA [10], GST–dMT [11], QsMT [18,19], cicMT2 [20] and ClMT2 [17].

(CCiT) de la Universitat de Barcelona (ICP-AES, DNA sequencing) and the Servei d'Anàlisi Química (SAQ) de la Universitat Autònoma de Barcelona (CD, UV–Vis, ESI-MS) for allocating instrument time.

Appendix A. Supplementary data

Supplementary data to this article can be found online at http://dx.doi.org/10.1016/j.jinorgbio.2015.02.016.

References

[1] M. Margoshes, B.L. Vallee, J. Am. Chem. Soc. 79 (1957) 4813–4814.
[2] E. Freisinger, Dalton Trans. (2008) 6663–6675.
[3] M. Capdevila, R. Bofill, Ò. Palacios, S. Atrian, Coord. Chem. Rev. 256 (2012) 46–62.
[4] http://www.bioc.unizh.ch/mtpage/classif.html (accessed July 8th, 2013).
[5] L. Hanley-Bowdoin, B.G. Lane, Eur. J. Biochem. 135 (1983) 9–15.
[6] C. Cobbett, P. Goldsbrough, Annu. Rev. Plant Biol. 53 (2002) 159–182.
[7] E.A. Peroza, R. Schmucki, P. Güntert, E. Freisinger, O. Zerbe, J. Mol. Biol. 387 (2009) 207–218.
[8] J. Loebus, E.A. Peroza, N. Bluthgen, T. Fox, W. Meyer-Klauke, O. Zerbe, E. Freisinger, J. Biol. Inorg. Chem. 16 (2011) 683–694.
[9] O.I. Leszczyszyn, H.T. Imam, C.A. Blindauer, Metallomics 5 (2013) 1146–1169.
[10] A.M. Tommey, J. Shi, W.P. Lindsay, P.E. Urwin, N.J. Robinson, FEBS Lett. 292 (1991) 48–52.
[11] K. Bilecen, U.H. Ozturk, A.D. Duru, T. Sutlu, M.V. Petoukhov, D.I. Svergun, M.H. Koch, U.O. Sezerman, I. Cakmak, Z. Sayers, J. Biol. Chem. 280 (2005) 13701–13711.
[12] R.M. Nezhad, A. Shahpiri, A. Mirlohi, Protein J. 32 (2013) 131–137.
[13] O. Schicht, E. Freisinger, Inorg. Chim. Acta 362 (2009) 714–724.
[14] M.A. Pagani, M. Tomas, J. Carrillo, R. Bofill, M. Capdevila, S. Atrian, C.S. Andreo, J. Inorg. Biochem. 117 (2012) 306–315.
[15] J. Guo, L. Xu, Y. Su, H. Wang, S. Gao, J. Xu, Y. Que, Biomed. Res. Int. (2013). http://dx.doi.org/10.1155/2013/904769.
[16] H.L. Wong, T. Sakamoto, T. Kawasaki, K. Umemura, K. Shimamoto, Plant Physiol. 135 (2004) 1447–1456.
[17] K. Akashi, N. Nishimura, Y. Ishida, A. Yokota, Biochem. Biophys. Res. Commun. 323 (2004) 72–78.
[18] G. Mir, J. Domènech, G. Huguet, W.J. Guo, P. Goldsbrough, S. Atrian, M. Molinas, J. Exp. Bot. 55 (2004) 2483–2493.
[19] J. Domènech, R. Orihuela, G. Mir, M. Molinas, S. Atrian, M. Capdevila, J. Biol. Inorg. Chem. 12 (2007) 867–882.
[20] X. Wan, E. Freisinger, Metallomics 1 (2009) 489–500.
[21] Food and Agriculture Organization of the United Nations, FAO, Statistical Yearbook 2013, World Food and Agricultura, Rome, 2013. 134.
[22] P. Madejón, J.M. Murillo, T. Marañón, F. Cabrera, M.A. Soriano, Sci. Total Environ. 307 (2003) 239–357.
[23] R. Herzig, E. Nehnevajova, C. Pfistner, J.P. Schwitzguebel, A. Ricci, C. Keller, Int. J. Phytorem. 16 (2014) 735–754.
[24] D. Mani, B. Sharma, C. Kumar, N. Pathak, S. Balak, Int. J. Phytorem. 14 (2012) 235–246.
[25] K.J. Livak, T.D. Schmittgen, Methods 25 (2001) 402–408.
[26] D. Mumberg, R. Müller, M. Funk, Gene 156 (1995) 119–122.
[27] V.C. Culotta, W.R. Howard, X.F. Liu, J. Biol. Chem. 269 (1994) 25295–25302.
[28] C.W. MacDiarmid, L.A. Gaither, D. Eide, EMBO J. 19 (2000) 2845–2855.
[29] O. Palacios, A. Pagani, S. Pérez-Rafael, M. Egg, M. Höckner, A. Brandstätter, M. Capdevila, S. Atrian, R. Dallinger, BMC Biol. 9 (2011) 4.
[30] T. Stearns, H. Ma, D. Botstein, Methods Enzymol. 185 (1990) 280–297.
[31] M. Capdevila, N. Cols, N. Romero-Isart, R. González-Duarte, S. Atrian, P. González-Duarte, Cell. Mol. Life Sci. 53 (1997) 681–688.
[32] J. Domènech, G. Mir, G. Huguet, M. Molinas, M. Capdevila, S. Atrian, Biochimie 88 (2006) 583–593.
[33] N. Cols, N. Romero-Isart, M. Capdevila, B. Oliva, P. Gonzàlez-Duarte, R. Gonzàlez-Duarte, S. Atrian, J. Inorg. Biochem. 68 (1997) 157–166.
[34] J. Bongers, C.D. Walton, D.E. Richardson, J.U. Bell, Anal. Chem. 60 (1988) 2683–2686.
[35] M. Capdevila, J. Domènech, A. Pagani, L. Tío, L. Villarreal, S. Atrian, Angew. Chem. Int. Ed. Engl. 44 (2005) 4618–4622.
[36] M. Tomas, M.A. Pagani, C.S. Andreo, M. Capdevila, R. Bofill, S. Atrian, J. Biol. Inorg. Chem. 19 (2014) 1149–1164.
[37] G. Zhou, Y. Xu, J. Li, L. Yang, J.Y. Liu, J. Biochem. Mol. Biol. 39 (2006) 595–606.
[38] http://www.heliagene.org (last accessed October 2014).
[39] N.H. Roosens, R. Leplae, C. Bernard, N. Verbruggen, Planta 222 (2005) 716–729.
[40] P. Kille, D.R. Winge, J.L. Harwood, J. Kay, FEBS Lett. 295 (1991) 171–175.
[41] Y. Wang, D. Hess, P.E. Hunziker, J.H.R. Kägi, Eur. J. Biochem. 241 (1996) 835–839.
[42] C. Gruber, S. Stürzenbaum, P. Gehrig, R. Sack, P. Hunziker, B. Berger, R. Dallinger, Eur. J. Biochem. 267 (2000) 573–582.
[43] P.J. Hensbergen, M.H. Donker, P.E. Hunziker, R.C. van der Schors, N.M. van Straalen, Insect Biochem. Mol. Biol. 31 (2001) 1105–1114.
[44] J.L. Bowman, S.G. Mansfield, in: J.L. Bowman (Ed.), Arabidopsis: An Atlas of Morphology and Development, Springer, New York, 1993, pp. 351–361.
[45] http://bar.utoronto.ca/efp/cgi-bin/efpWeb.cgi (last accessed January 2015).
[46] A.I. Mantese, D. Medan, A.J. Hall, Ann. Bot. 97 (2006) 999–1010.
[47] E.A. Peroza, E. Freisinger, J. Biol. Inorg. Chem. 12 (2007) 377–391.
[48] O.I. Leszczyszyn, R. Schmid, C.A. Blindauer, Proteins 68 (2007) 922–935.
[49] X. Wan, E. Freisinger, Inorg. Chem. 52 (2013) 785–792.
[50] T. Huber, E. Freisinger, Dalton Trans. 42 (2013) 8878–8889.
[51] E.A. Peroza, A. dos Santos Cabral, X. Wanz, E. Freisinger, Metallomics 5 (2013) 1204–1214.
[52] S. Perez-Rafael, A. Pagani, O. Palacios, R. Dallinger, M. Capdevila, S. Atrian, ZAAC 639 (2013) 1356–1360.
[53] R. Palmiter, Proc. Natl. Acad. Sci. U. S. A. 95 (1998) 8428–8430.